OPEN ACCESS



NGC 6302: The Tempestuous Life of a Butterfly

Bruce Balick¹, Lars Borchert², Joel H. Kastner³, Adam Frank⁴, Eric Blackman⁴, Jason Nordhaus^{5,6}, and Paula Moraga Baez⁷

Patha Moraga Baez

Department of Astronomy, University of Washington, Seattle, WA 98195-1580, USA; balick@uw.edu

Department of Physics and Astronomy, Aarhus University, Ny Munkegade 120, DK-8000 Aarhus C, Denmark; larseric@post.au.dk

Center for Imaging Science and Laboratory for Multiwavelength Astrophysics, Rochester Institute of Technology, Rochester, NY 14623, USA; jhk@cis.rit.edu

Department of Physics & Astronomy, University of Rochester, Rochester, NY 14627, USA; blackman@pas.rochester.edu

Center for Computational Relativity and Gravitation, Rochester Institute of Technology, Rochester, NY 14623, USA; jtnsma@rit.edu

National Technical Institute for the Deaf, Rochester Institute of Technology, NY 14623, USA

School of Physics and Astronomy and Laboratory for Multiwavelength Astrophysics, Rochester Institute of Technology, USA

Received 2023 March 28; revised 2023 August 8; accepted 2023 August 27; published 2023 October 27

Abstract

NGC 6302 (The Butterfly Nebula) is an extremely energetic and rapidly expanding bipolar planetary nebula (PN). If the central source is a single star, then its apparent location in an H-R diagram places it among the most massive, hottest, and presumably rapidly evolving of all central stars of PNe. Our proper motion study of NGC 6302, based on Hubble Space Telescope WFC3 images spanning 11 yr, has uncovered at least four different pairs of uniformly expanding internal lobes ejected at various times and orientations over the past two millennia at speeds ranging from 10–600 km s⁻¹. In addition, we find a pair of collimated off-axis flows in constant motion at \sim 770 \pm 100 km s⁻¹ within which bright [Fe II] *feathers* are conspicuous. Combining our results with those previously published, we find that the ensemble of flows has an ionized mass >0.1 M_{\odot} and its kinetic energy, between 10^{46} and 10^{48} erg, lies at the upper end of gravity-powered PNe ejection processes such as stellar mergers or mass accretion. We assemble our results into a plausible historical timeline of ejections from the nucleus and suggest that the ejections are powered by gravitational infall.

Unified Astronomy Thesaurus concepts: Planetary nebulae (1249); Bipolar nebulae (155); Ejecta (453); Stellar wind bubbles (1635); Shocks (2086)

1. Introduction

NGC 6302 (aka "The Butterfly") is an unusually active and large bipolar planetary nebula (PN) that is powered by an energetic but unseen central source (CS 8). As illustrated in Figure 1 and noted by Aller et al. 1981, NGC 6302 is a PN whose "appearance suggests violent motions with some bilateral symmetry." Hubble Space Telescope (HST) images found in our previous papers on NGC 6302, Kastner et al. (2022a, 2022b, hereafter K+22a,b), revealed that the geometric simplicity of the outlines of its lobes (wings) belie the complex structure and dynamics within their interiors, as first noted by Meaburn & Walsh (1980a, 1980b, hereafter M+80a, M+80b). Moreover, as we show later, the large mass of the ionized nebula, $M_{\rm neb}$, stellar mass injection rate, M, stellar wind speed, $\nu_{\rm wind}$, and the numbers of distinct flows of distinct ages in the wings are unusually large among bipolar PNe.

K+22a presented and discussed a suite of deep and panchromatic HST of NGC 6302 taken with the Wide Field Camera 3 (WFC3) in 2019–2020. As they noted, the nebula separates into an inner core of radius $\sim 15''$ and two larger

Original content from this work may be used under the terms of the Creative Commons Attribution 4.0 licence. Any further distribution of this work must maintain attribution to the author(s) and the title of the work, journal citation and DOI.

lobes, or butterfly *wings* to the E and W (E and W wings; Figure 1.) This paper focuses on the structures and proper motions within the wings of NGC 6302 that have been uncovered since K+22a, b were published as well as their evolutionary implications.

The morphologies of the structures in the wings (projected onto the sky) cleave into opposed pairs of wedges, as shown in Figure 1. The largest and optically brightest wedge pair consists of an array of edge-brightened clumps with radial tails that give the nebula its violent appearance (see Aller et al.). Additionally, the pair of [Fe II] wedges contain a prominent pair of feather-shaped radial [Fe II] features ([Fe II] feathers) and shocked features around the nebular core. Seemingly empty gaps lie along the symmetry axes of the large and seemingly hollow *northwest breakout lobe* (NWBL; K+22a) that extends beyond the WFC3 field of view (Figure 2(a)) as well as a possible SE counterpart.

The goal of this paper is to combine our HST observations with previously published information to explore the nebula's unusually complex history and evolution. The WFC3 images of K+22a and the proper motion studies that comprise the foundation of this study are presented in Section 2. In Section 3, we describe additional significant properties of NGC 6302 based on a further analysis of the images from K+22a and previous results in the literature. In Section 4, we explore the formation, internal pressures, energetics, and mass injection rates into the wings. In the final section, we review plausible mass ejection processes from the unusually massive and powerful CS.

⁸ CS often denotes "central star" in papers like this one. We use CS to represent central source—a functional term that connotes a generic central engine that creates outflows of sundry mass flux, momentum, shape, and orientation—possibly intermittently. We adopted "central source" in order to account for the complexity of the nebular structure and dynamics the central source may be a binary or multiple star system, possibly with internal mass flows and accretion disks. The properties of the CS are reviewed in K+22a.

 $[\]frac{9}{\text{As discussed in K+22a, [Fe II] emission is a standard tracer of relatively J-type shocks at speeds <math>v_s \ge 50-100 \text{ km s}^{-1}$.

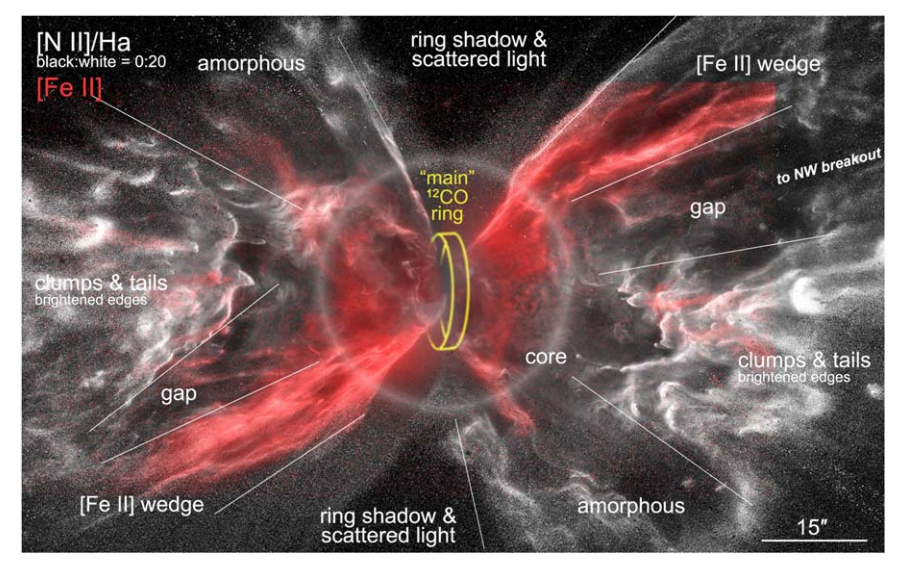


Figure 1. A modified version of Figure 5 in K+22a that identifies morphologically distinct wedges within the bipolar wings of NGC 6302 as seen in contrast-enhanced versions of [Fe II] (red) and [N II]/H (gray) images. Various significant zones beyond the core (gray circle) are identified. A schematic of the *main* equatorial CO ring from S-G+17 has been aligned to the HST images. North is up.

2. Zones of Coherent Motions

This section focuses on structure and associated changes within the wings of NGC 6302 between 2009 and 2020 as can be seen in the WFC3 camera and F658N images and related results derived directly from the HST data. Our primary results are compiled in Figures 2 and 3. Both are montages of panels within which we arranged to facilitate comparisons of the same nebular regions of the nebula in different WFC3 images and image ratios. The reader is referred to K+22a for a description of these images and their calibrations. Hereafter, we adopt a distance $D_{\rm kpc}=1$ to NGC 6302 (K+22a, Gómez-Gordillo et al. 2020), so each pixel, 0."0396, covers ~40 AU.

2.1. Proper Motions

The results of the present proper motion studies were extracted from HST F658N images from 2009 and 2020 in which nebular features are the sharpest and brightest (see also Rauber et al. 2014, hereafter R+14). The two-epoch images were aligned by sub-pixel translations of the 2009 image relative to an expansion center that was determined by trial and error. We initially applied the *difference method* (Reed et al. 1999) to trace their 11 yr proper motions. In that method, *residual images* are created from the differences of the original pair of images after a magnification factor *M* is applied to the 2009 images. If the nebula expands uniformly then the residual image will be null other than noise, camera imperfections, and field stars.

We also used a similar methodology, the *ratio method*, in which the aligned two-epoch images are divided. Although the two methods yield equal values of M and its uncertainties in bright regions, we preferred the ratio method since signals of change are much more readily apparent for structures of low surface brightness. The raw signals of proper motions (before applying any magnification to the 2009 image) are shown in Figure 2(c). Leading white and trailing black patterns on opposite sides of thin features are the usual signs of displacements. White (black) pixels have values of 1.5 (0.5), so the signals of proper motion are readily visible above the noise level.

Figure 2(d) shows the smallest residuals in zones (outlined in colors) after the best local value of M has been applied. Red lines outline one pair of zones in which the ratio method could not satisfactorily null the residuals—that is, the structures in this zone do not expand uniformly (Figures 3(a)–(c)).

2.2. Zones of Uniform Expansion

Zones of uniform expansion (ZUEs) in NGC 6302 consist of distinct ensembles of clumps or thin features whose overall expansion is characterized by the same radial speed gradient i.e., expansion age. However, no single magnification factor nulls the residuals of all of the structures throughout the wings. To explore the expansion patterns further, one of us (L.B.) made a movie of the residuals of ratio images in which M increases from 1.0000 to 1.0160 in increments of 0.00143. We were able to find distinct values of M that successfully null the residuals within each of several ZUEs depicted with black lines in Figure 2(d). The resulting values of $M_{\rm ZUE}$ are listed in Table 1, where, for each ZUE, we show the corresponding expansion ages, Δt_{ZUE} , radii, θ_{tip} , and proper motion speeds, $v_{\rm tip}$, at their leading tips. Note that values of $\Delta t_{\rm ZUE}$ are independent of flow inclination. The speed gradients within each of the ZUEs are listed for later comparison to earlier estimates in the literature based on long-slit spectra.

As expected for bipolar PN, the ZUE's generally come in zonal pairs in opposite directions with one exception—the innermost ZUE immediately east of the center—whose western counterpart is likely to be obscured by strong foreground dust extinction in the vicinity (K+22a).

We checked the F658N results of proper motions in the zonal expansions against our two-epoch F656N and F673N pairs, respectively. All outcomes are in good agreement, although the signal-to-noise ratio of the F658N images is at least twice as large. These proper motions agree, on the whole, with the independent estimates of the aggregate proper motions within the core made from 2009 and 2019 WFC3 images of F673N by K+22a (Figure 11). They are also consistent with earlier studies of larger uncertainties by Meaburn et al. (2008, hereafter M+08) and Szyszka et al. (2011).

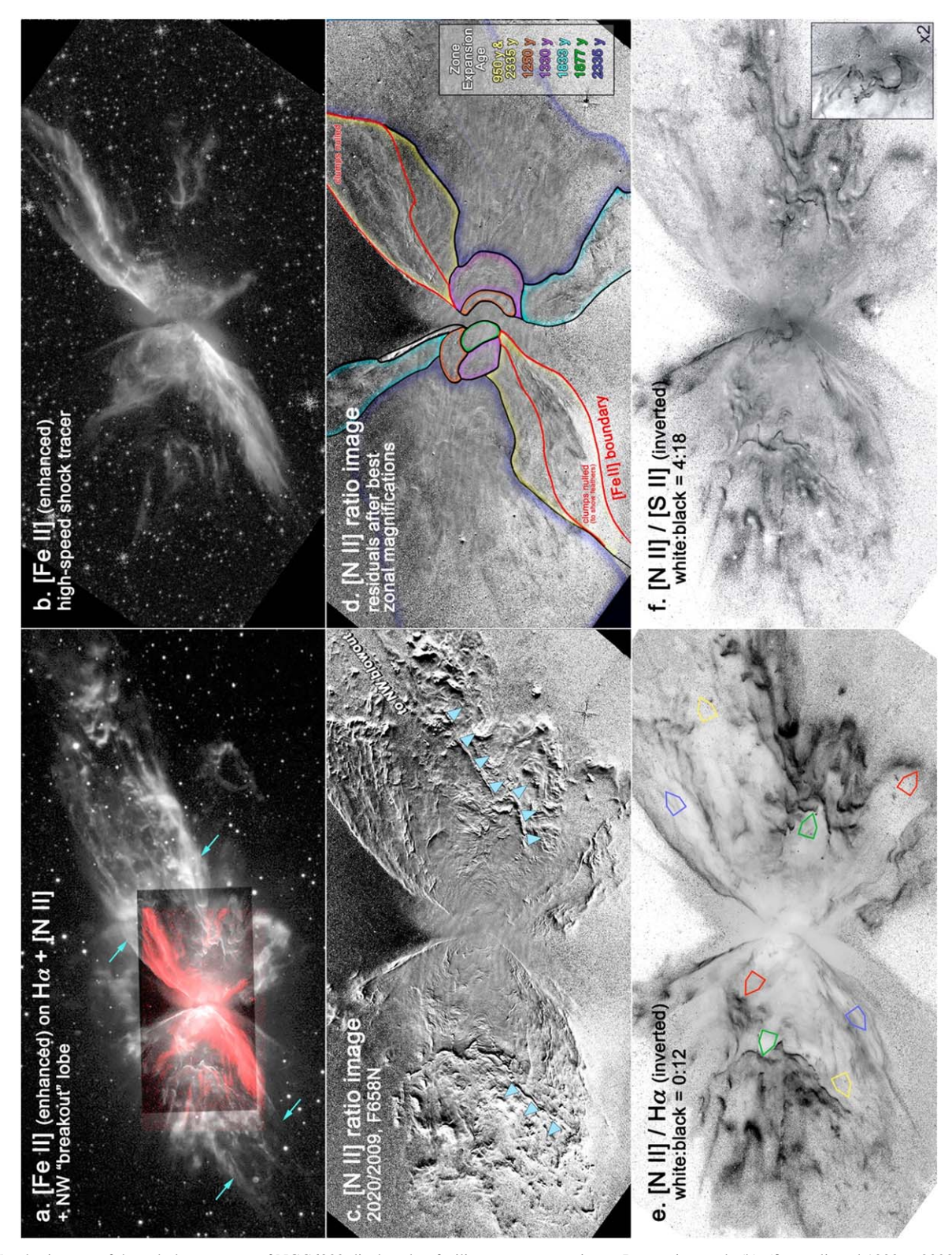


Figure 2. Sundry images of the nebular structure of NGC6302 displayed to facilitate easy comparisons. Images in panels (b)–(f) are aligned 1000×2000 portions of HST images displayed at 0.0000 pixel. North is up. Panel (a) shows a deep wide-field 10000 pixel pix

2.3. Zones of Uniform Translation

The residuals of the 2019/2009 F658N ratio within the red zones of Figure 2(d) cannot be flattened for any value of M_{ZUE} .

That is, they show an ensemble of string-like features in the residual images that steadily shift in radius as M is incremented (Figures 3(a)–(c)). Nevertheless, an excellent null is obtained

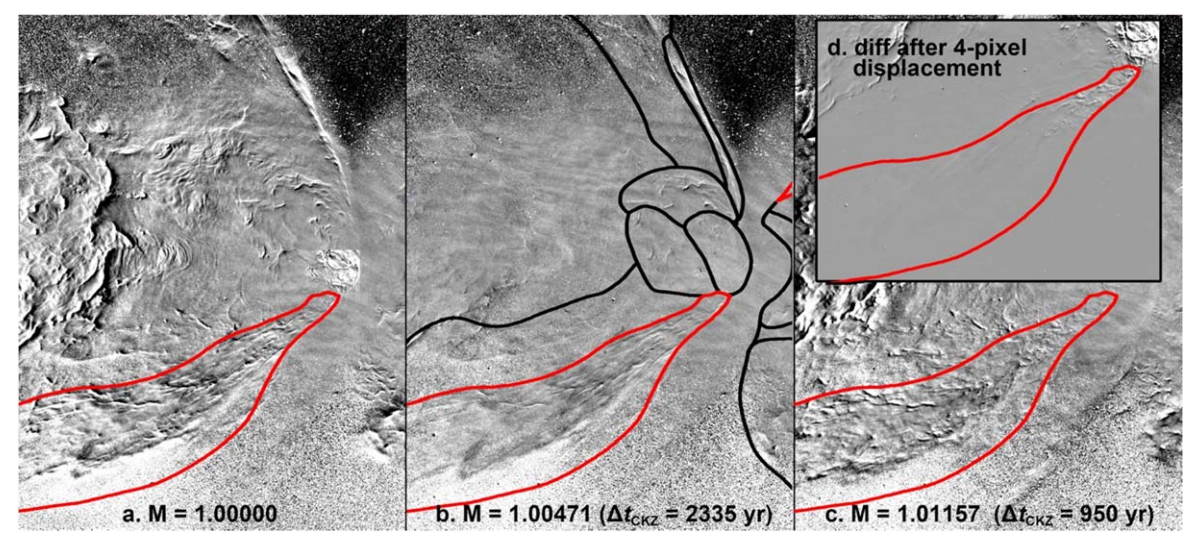


Figure 3. Panels (a)—(c) show the residuals in the eastern portions of the 2020 and 2009 F658N image ratios after the latter has been magnified by a factor of *M* and divided by the former. Those features that share a common magnification (aka expansion age) are nulled if *M* is successfully chosen; however, no value of *M* nulls the full set of sinewy features in the red zone. (Faint horizontal waves are artifacts imposed by internal reflections in the filter.) Panel (d) The pattern of the residuals in the red zone after a 4.0 pixel radial translation of the 2009 image relative to that of 2019 (see the text).

Table 1
Fitted Parameters of the ZUEs

Best M _{ZUE} —1 (Uncertainty)	$\Delta t_{\rm ZUE}$ (yr)	$\theta_{\rm tip} \pm 30\%$ (")	$v_{\rm tip} \pm 30\% ~({\rm km~s^{-1}} ~{\rm in} ~{\rm the} ~{\rm Sky} ~{\rm Plane})$	Speed Gradient $v_{\rm tip}~({\rm km~s}^{-1})/\theta_{\rm tip}~('')$
0.00471 (10%)	2335	177 ^a	360	2.0 ^b
0.00586 (20%)	1877	45	113	2.7
0.00600 (10%)	1833	5.2	13	2.9
0.00786 (20%)	1330	20	68	3.5
0.00914 (10%)	1250	15	60	4.0

Notes.

by subtracting the two-epoch image pair after applying a small radial translation of the earlier image by $\Delta r = 4.0 \pm 0.5$ pixels (Figure 3(d)). This translation corresponds to a constant radial speed of $770 \pm 100 \, \mathrm{km \, s^{-1}}$ in the sky plane for $D_{\mathrm{kpc}} = 1$. This flow began $\sim\!300$ yr ago since the leading edges of the zones of uniform translation (ZUTs) lie at a projected angular radii of $\sim \pm 45''$ from the nucleus. It is interesting that the ZUTs emanate from opposite edges of the dense, slowly expanding CO main ring (Santander-García et al. 2017, hereafter S-G+17) shown schematically in Figure 1, as if this ring inertially confines their orientation. The closest counterparts of the ZUT feature in the [Fe II] wedges are shocked knots within the jets of Herbig–Haro (HH) objects (Erkal et al. 2021).

3. Other New Results

3.1. Outflow Mass, Energetics, and Ionization

Most of the total mass of the ionized lobes, $M_{\rm neb}$, appears to be in the clumps E and W of the CS. An estimate of $M_{\rm neb}$ is a key step in understanding the kinetic energy of the nebular gas. However, as discussed by K+22a, published nebular mass estimates are highly discordant. Given the large range in these mass estimates, we shall adopt $M_{\rm neb} = 0.1~M_{\odot}$. Therefore, the mass injection rate from the CS is $M_{\star} \approx M_{\rm neb}/\Delta t_{\rm ZUE} \approx 4 \times 10^{-4}~M_{\odot}~{\rm yr}^{-1}$ if we assume that $\Delta t_{\rm ZUE} \approx 2300~{\rm yr}$ for the clumps. For comparison, M+80a, b, Matsuura et al. (2005),

Dinh-V-Trung et al. 2008, M+08, Szyszka et al. (2011), S-G+17, and Bollen et al. 2020) all estimated $M_{\star} \ge 10^{-4} M_{\odot} \text{ yr}^{-1}$ (at $D_{\text{kpc}} \sim 1$). These values of M_{\star} are all larger than estimates of mass loss from typical AGB stars, $\approx 10^{-5} M_{\odot} \text{ yr}^{-1}$ (Höfner & Olofsson 2018).

The total kinetic energy within the nebular wings is $E_{\rm neb} = 1/2\,M_{\rm neb}\,v_{\rm neb}^2$, where $v_{\rm neb}$ is the speed of the complex network of internal flows. If we adopt conservative representative values for $v_{\rm neb} = 100\,{\rm km~s^{-1}}$, then $E_{\rm neb} = 10^{46}$ erg. $E_{\rm neb}$ increases to 10^{48} erg if we adopt $M_{\rm neb} = 1.3\,M_{\odot}$ (Wright et al. 2011) and $v_{\rm neb} = 268\,{\rm km\,s^{-1}}$ as measured at point A near the midpoint of the NWBL (M+05). The total flow energy injected from the CS can be greater if winds escape through gaps in the wings.

The ionization of PNe is normally dominated by stellar UV photons (Dopita & Sutherland 1996). Given the location of the CS in the H-R diagram, we can assume that this is also the case throughout much of NGC 6302. However, shocks also locally contribute to the ionization and total thermal energy of NGC 6302. M+80a, b were the first to mention shock heating in its wings and the NWBL. L+19 suggested that the line fluxes that arise in the outer wings are primarily the result of shocks. In section 4 we shall show that shocks permeate the nebula.

3.2. The NW Gap and Breakout Lobe

The edges of the dynamically coherent NWBL (Figure 2(a)) can be traced from the core to well outside the wings of NGC

^a Tip of NWBL (knot 1 of M+08).

b In good agreement with proper motion studies of knots by Meaburn et al. (2005, hereafter M+05) and Lago et al. (2019, hereafter L+19).

6302 and beyond the field of view of the WFC3 camera. The morphology and dynamics of the NWBL were mapped by M+05 and M+08 who found that it extends fully 2'.95 from the nucleus (0.86 pc at $D_{\rm kpc}=1$). They found that the NWBL expands uniformly at $\sim\!0.5$ mas yr $^{-1}$ per arcsec ($\sim\!2.5\,{\rm km\,s}^{-1}$ arcsec $^{-1}$ at $D_{\rm kpc}=1.0$) with a speed of $\sim\!600\,{\rm km\,s}^{-1}$ at its leading tip. The speed gradient (aka expansion age) of the NWBL is similar to that of the adjacent ZUE formed by the clumps (Table 1). Thus, the NWBL and the clumps may have been formed in the first and most energetic of a series of mass ejection events that started $\sim\!2300$ yr ago.

The seemingly hollow NW gap lies along the symmetry axis of the NWBL and appears to spatially connect it to the core (Figure 2(a)). The NW gap is bounded by compressed ridges of H_2 on one side (Davies et al. 2003) and [Fe II] on the opposite side, both of which expand laterally and join the lateral edges of the NWBL at its base (Figure 2(c); see also the SHAPE model¹¹ in Figure 15 of M+05). Plausibly the 770 km s⁻¹ flow through the [Fe II] feather plays some sort of role in the energetics of the NWBL.

The kinematic age of the NWBL makes it one of the youngest lobes in any large ($\sim 1~\rm pc)$ bipolar PN, including Hen 2-111 (age $\sim 8~\rm kyr$, Dopita et al. 2018), NGC 1360 (age $\sim 10~\rm kyr$; García-Díaz et al. 2008; López et al. 2008), and A63 (age $\sim 18~\rm kyr$, Walton et al. 1993). For comparison, typical compact PNe with collimated flows grow at $\leq 10\%$ of the tip speed of the NWBL (e.g., Rechy-García et al. 2020). Its tip speed renders the NWBL the fastest of the lobes in these other large bipolar PNe such as NGC 2440 (Lago & Costa 2016).

3.3. The Bubble in the Inner Core

One of the most unusual features of NGC 6302 (and every other PN) lies deep in the core of the high-ionization core region of NGC 6302 in which He II and [Ne V] reach their nebular peak brightness (R+14; K+22a, respectively). The outer edge-brightened ring that surrounds this *inner bubble* (inset of Figure 2(f)) of radius $\sim\!0.02$ pc attaches to the equator of the dense, cold, and slowly expanding main ring of ^{12}CO that bisects the wings (S-G+17). The bubble and the adjacent main ^{12}CO ring share the same expansion age as the prominent clumps and tails $\pm30''$ to its E and W as well as the NWBL, so all of them may have been formed together.

The ionization of the ring of the inner bubble is anomalous. It is prominent in images of the molecules of ^{12}CO , H_2 as well as HST images of the ionic lines of [S II], [N II], $\text{H}\alpha$, $\text{H}\beta$, [O iii], and He II λ 4686 Å. Its unresolved leading rim is visible in these species whose ionization potentials range of range from $\sim\!10\,$ eV in the molecules to 54 eV in He II. This 1 pixel width, $\sim\!50\,\text{au}$, is consistent with the leading edge of a radiative shock. 12 However, the rim is not visible [Fe II]. (The brightnesses of the bluest images of the core region surrounding the bubble are likely modulated by deep and patchy foreground dust and contaminated by scattered light from the nebular center.)

4. Internal Dynamics

The structures and motions within the wings of NGC 6302 are among the most complicated of any PN, consistent with a complex history of mass ejection and shaping. Shaping begins at ejection; however, additional shaping ensues as internal thermal and ram pressures exert their influences. We next infer the shaping mechanisms within the wings of NGC 6302 based on our results in the two previous sections.

4.1. Shock Tracers in NGC 6302

The patterns of pressures and flows are clearly complex and projected onto the sky. Nonetheless, other than ionization fronts (IFs), radiation cannot create the messy network of tangled filaments. Generally, lobes will be outlined by readily recognizable radiative shocks whether inflated by invisible fast winds (e.g., Lee & Sahai 2003, Balick et al. 2018, 2019) or the thermal pressures of hot gas (e.g., Icke et al. 1992). We posit that most or all of the sinewy filaments seen in [Fe II], H_2 , [N II]/ $H\alpha$, and [N II]/[S II] trace the visible interfaces within the wings of NGC 6302 at thin interfaces¹³ where fast winds or hot gas interact with ambient gas or each other.

[N II]/H α and [S II]/H α ratios are good J-type shock tracers since the forbidden lines are enhanced in the recombination zones associated where gas compression boosts the recombination rates of ionized species (e.g., Hartigan et al. 1994; Dopita 1997; Raga et al. 2008). Both the [N II] and [S II] lines may be excited ionized by UV photons created in situ by high-velocity (>100 km s⁻¹) radiative shocks (Dopita 1995), such as those found in SN 1987A (McCray & Fransson 2016) and LINERS (Heckman 1980a, 1980b). Figure 2(e) shows that this is almost certainly the case for [N II]/H α in NGC 6302.

Like [N II], H_2 is also an excellent tracer of shocks along the inner edges of bipolar lobes (Kastner et al. 1996; Guerrero et al. 2000; Fang et al. 2018) where stellar photon fluxes are reduced by their highly oblique incidence. Similarly, where it is detectable, shock-excited [Fe II] λ 16400Å emission is well known to trace shock interfaces in which $v_{\rm shock} \geq 50~{\rm km~s^{-1}}$, especially in HH objects (Erkal et al. 2021), interstellar bullets (Bally et al. 2020), supernova remnants (Keohane et al. 2007), and active galactic nuclei (Forbes & Ward 1993). Contini et al. (2009) argued that [Fe II] emission is emitted only where $n_e > 10^6~{\rm cm^{-3}}$. In this case, the corresponding Fe⁺ recombination time $\approx (10^5~{\rm yr})/n_e \approx 1~{\rm month}$, so the largely radial [Fe II] filaments in NGC 6302 must be sustained by strong lateral pressure gradients.

In addition, as we argue in Appendix, filamentary enhancements of the [N II/[S II] ratio trace compressed gas that arise in recombination zones behind shocks where $n_e > 10^4$ cm⁻³. This high-density tracer is easily measured throughout the lowionization outer wings of NGC 6302 where other high-density tracers of much higher ionization, e.g., [Ar IV], are not detectable (R+14). The origin of the dense low-ionization filaments can only be J-type shocks (K+22a).

Interestingly, the [N II] and H₂ filaments do not have apparent coincident [Fe II] counterparts and vice versa. This can be explained if $n_e \gg n_{\rm crit}({\rm [N~II]})$ in the [Fe II] emission

¹⁰ Its thin, fragmented edges suggest that they have undergone rapid radiative cooling since they formed (Pittard et al. 2005).

¹¹ SHAPE (Steffen et al. 2011) is a heuristic modeling tool for generating three-dimensional models of expanding nebula assuming that their expansions are uniform.

 $^{^{12}}$ Image references are K+22a except for 12 CO (S-G+17), H₂ (Davies et al. 2003), and He II (Noll, 2009).

 $[\]overline{13}$ For strong J-type shocks, the cooling time, $t_{\rm cool}\approx 10^4$ yr $(v_{\rm shock}/100)\,{\rm km~s^{-1}}/(n_{\rm H,0}~{\rm cm^{-3}})$ yr, where $v_{\rm shock}$ is the shock speed and $n_{\rm H,0}$ is the preshock density $(\sim 1/4~n_{\rm wind})$. The shock thickness is given by $L_{\rm cool}=^{1/4}v_{\rm shock}~t_{\rm cool}$ (Draine 2011). For $n_{\rm H,0}\sim 10^3~{\rm cm^{-3}}$ and $v_{\rm shock}\sim 100~{\rm km~s^{-1}}$, $t_{\rm cool}\approx 10$ yr and $L_{\rm cool}\sim 50~{\rm au}\sim 1~{\rm WFC3}$ pixel at $D_{\rm kpc}=1$.

zone, as asserted by Contini et al. Here $n_{\rm crit}([{\rm N~II}]) \sim 8 \times 10^4 \, {\rm cm}^{-3}$ is the *critical density* at which the $[{\rm N~II}] \, \lambda 6548 {\rm Å}$ line is de-excited at equal rates by radiative emission and collisional thermalization (Draine 2011).

In corroboration, L+19 have argued that UV photons from the CS are too dilute in the outer wings of NGC 6302 to explain the observed fluxes of [S II] and [N II] from IFs. They concluded that shocks must dominate local excitation. R+14 came to the same conclusion for other reasons.

4.2. Shaping

Other clues to the nature of shock excitation are provided by the internal morphology within the wings of NGC 6302. One of the most striking of these are cone-shaped features associated with invisible and highly collimated flows (jets) that have burrowed into the nebula (e.g., colored pointers in Figure 2(e)). Also, the pair of ZUTs that are surrounded by bright [Fe II] lines are another example of jets that are actively shaping their surroundings. Patches of [Fe II] elsewhere give the impression that fast winds from the core irregularly permeate beyond the core (Barral et al. 1982).

Jets may have initially formed these intrusions. However, there is little evidence that these intrusions are presently sustained by jets (with the exception of the ZUTs). The shapes and overall expansion pattern of the intrusions can persist long after the momentum flux of the jet abates provided that the leading edge of the intrusion is not retarded by downstream gas (Huarte-Espinosa et al. 2012; Balick et al. 2019). Thus, the growth of the intrusions can be ballistic or driven by the thermal pressure of hot gas from the core where fast stellar winds thermalized. The latter is analogous to the numerous hot, soft X-ray *bubbles* in the interiors of many elliptical PNe (Kastner et al. 2012, Toalá & Arthur 2018).

Other conspicuous clues are the shocked radial tails behind many of the more distant clumps in the wings E and W of the CS (Figure 2(e),(f)). The tails appear to be gas that has been ablated from the small clumps and swept outward by winds or flows from the nebular core (Steffen & López 2004; Raga et al. 2005; Toalá & Arthur 2011; Toalá & Arthur 2014).

Davis et al. (2003) found that the brightest H_2 beyond the core of NGC 6302 lies along a pair of ridges on one edge of both gap wedges. The pair of [Fe II] feathers—each with fast radial flows through their interiors—are found on the opposite sides of both gaps. These H_2 ridges and [Fe II] feathers outline the respective bases of pairs of large and laterally expanding lobes, as indicated by the cyan triangles in Figure 2(c). This suggests that the gaps are inflated by hot gas and delineated by thin, shock-compressed neutral gas. We surmise that the seemingly hollow NWBL might be filled with hot gas in transit from the core. There may be a counterflow through the opposite gap wedge in the SE.) Unfortunately, however, Davis et al. (2003) were unable to determine the nature of the H_2 excitation from their spectra.

M+05 concluded that the growth of the NWBL results either from the ongoing ram pressure of radial winds from the CS (e.g., Barral & Cantó 1981) or ballistic expansion. We favor a hybrid model in which the basic shape of the NWBL was formed by a fast jet $\sim\!2300$ yr ago. Thermal pressure or ballistic

growth may now sustain the expansions of its walls and lateral edges.

5. Conclusions

Aller et al. (1981) were correct: the wings of the Butterfly contain several highly energetic radial outflows. Our HSTbased proper motion study reveals that the wings of NGC 6302 contain multiple pairs of expanding lobe-like outflow structures ejected from the CS over the past two millennia, each with its own expansion speed, orientation, and perimeter shock. Most of the lobes expand uniformly—a common expansion pattern for PNe of all ages and shapes—at 2–4 km s⁻¹ arcsecond⁻¹, i.e., expansion ages between \sim 1200 and \sim 2300 yr. Additionally, as pairs of thin jets have been flowing into a pair of shocked [Fe II] feathers at \sim 770 km s⁻¹ for at least the past 300 yr. Another ZUE of age ~2300 yr, the NWBL, can be traced beyond the field of our HST images. Like other intrusions, it may have been formed initially by a collimated jet. However, the absence of a stream of shocked gas at the tip of the NWBL suggests that its present forward and lateral expansion is possibly ballistic or driven by the pressure or thermalized fast winds from the CS.

The optically brightest and most complex structures within the wings consist of ensembles of clumps (many with radial tails) $\pm 30''$ E and W of the core region. Their thin star-facing edges show very large and spatially variable [N II]/H α (from 2–15) and [N II]/[S II] ratios (from 4–18) in a complicated filamentary network. We interpret the filaments as the shocked interfaces resulting from the ram pressure of fast winds from the CS or the thermal pressure of hot ($\sim \! 10^7$ K) wind-heated gas. Bright H $_2$ is spatially correlated with shocked filaments of [N II]/ α , as commonly seen in other bipolar PNe (Guerrero et al. 2000). However, neither line correlates with [Fe II] emission, possibly because density in the [Fe II] region, n_e $> 10^6$ cm $^{-3}$, quenches [N II] and other common shock tracers.

This historical scenario of the formation and shaping history of the wings emerges:

- 1. $\sim 2300~yr~ago$. The first and most energetic of a series of ram-pressure-dominated and collimated outbursts from the CS formed the main equatorial molecular ring as well as some large and irregular groupings of clumps and other structures E and W of the nucleus. The star-facing edges of the clumps are readily observable in shock tracers, arguing that they are immersed in flows of winds or hot gas escaping from the core. The hollow NWBL that extends almost a parsec from the core and whose tip has a proper motion of $\sim 600~{\rm km~s^{-1}}$ is another feature created in this event.
- 2. Between ~1200 and 1900 yr ago. At least three weaker outburst events from the CS produced smaller pairs of opposite ZUEs into the wings along different symmetry axes. One of these is a small bright bubble adjacent to the equatorial disk is seen in molecular and ionic lines from emitting species with a huge range of ionization potentials, including ¹²CO, H₂, H I, and He II.
- 3. ~300 yr ago to the present. A pair of fast and ongoing jets from the CS lies within each of the bright pair of [Fe II] feathers. A network of thin, shocked, and largely radial [N II] features within each feather share common radial proper motion speeds of 770 km s⁻¹. The

 $[\]overline{\ }^{14}$ However, Casassus et al. (2000) and Oliva et al. (1996) argued that shocks are not important in NGC 6302. In this case, the formation of the [Fe II] features, the presence of thin of [N II]/Hα-enhanced filaments, and the causes of the patterns of proper motions of the ZUEs and the ZUT are not explained.)

symmetry axis of one of these flows aligns with the outer edge of the NWBL.

These events are seemingly connected to ejecta from at least one luminous and very hot central star as it traversed the H-R diagram. This central star is the primary source of nebular photoionization. Winds arising from this star and its nearby companions have been reshaping the wings of the nebula.

5.1. Formation and Ejection Paradigms

We explore how the constraints that nebular history imposes on paradigms of stellar mass ejection. We estimate the total kinetic energy of the outflows in the wings, $E_{\rm neb} = 1/2~M_{\rm neb}$ $v_{\rm neb}^2$, between 10^{46} and 10^{48} erg, and possibly more if mass has escaped from the wings. This energy is larger than the largest kinetic energies of the $^{12}{\rm CO}$ of many younger PNe, such as Frosty Leo, CRL 618, CRL 2688, and NGC 7027, as measured by Bujarrabal et al. (2001) from their $^{13}{\rm CO}$ and partially saturated $^{12}{\rm CO}$ line profiles.

It is clear that non-recurrent ejection mechanisms—such as binary-star mergers and common-envelope ejections (Zou et al. 2020; Glanz & Perets 2021a and García-Segura et al. 2022 and earlier papers in the series)—are not applicable. Typical, mass ejections from the active stellar surface of an AGB star, such as the recent SME of Betelgeuse (Dupree et al. 2022), fall short of accounting for the speeds and densities of the outbursts from the CS of NGC 6302 (see Jadlovský et al. 2023).

Gravitational infall is the most likely ultimate source of the large kinetic energies of the outflows I NGC 6302. Soker & Kashi (2012) and K+22a discussed the possibility of an *intermediate-luminosity optical transient event* in which mass from an AGB donor falls onto a companion main-sequence companion. An ILOT event releases a total kinetic energy of 10^{46} – 10^{49} erg. The ejection speeds, a few hundred kilometers per second, are consistent with the flow speeds that we found in the wings of NGC 6302. However, the brief duration and singular nature of ILOT events render this paradigm untenable.

Other gravitational paradigms are still being developed in the literature. An increasingly common one is that the orientation and kinetic energies of the flow pattern are influenced by multiple nearby companions and/or their related accretion flows, as invoked recently by De Marco et al. (2022) and Sahai et al. (2023) to explain the morphology of NGC 3132, and by Henney et al. (2021) to account for orientations and ages of five ejection events over the past \sim 3500 yr in NGC 6210. For similar reasons, K+22a suggested that stellar multiplicity is highly likely in NGC 6302 (K+22a). ¹⁵ We note that Feibelman (2001) suggested that the CS of NGC 6302 contains at least a G-type star and a white dwarf.

These or any other sort of explanation for the mass ejection of NGC 6302 will likely remain in the realm of speculation without better observational constraints on the so-far invisible CS. About all that we can state with some degree of confidence is that the star in the central engine that provides the bulk of the nebular ionization and kinetic energies of the outflows has a Zanstra temperature $>2\times10^5$ K and its luminosity lies between $10^{2.9}$ and $10^{4.4}$ L_{\odot} (K+22a). Our most pressing observational challenge is to better constrain our understanding of the nature of the star(s) in the core of NGC 6302.

Acknowledgments

We are grateful to Miguel Santander-García for helpful advice. The proper motion results in this paper are based on observations made with the NASA/ESA HST, obtained at the Space Telescope Science Institute (STScI), which is operated by the Association of Universities for Research in Astronomy, Inc., under NASA contract NAS5-26555. The 2019-2020 (2009) observations are associated with program GO15953 (GO 11504). J.H.K. and P.M.B. acknowledge the support provided by the U.S. National Science Foundation (NSF) grant AST-2206033 and NASA/STScI grant HST-GO-15953.001-A to the Rochester Institute of Technology. A.F. acknowledges the support of US Department of Energy grants DE-SC0001063 and DE-SC0020432 to the University of Rochester. E.B. acknowledges the support of NSF grants AST-1813298 and PHY-2020249. J.N. acknowledges support from grant NSF AST-2009713 to the Rochester Institute of Technology.

Data Availability

The HST data used in this study can be found in the Mikulski Archive for Space Telescopes (MAST): doi:10.17909/8139-0772

Appendix

In Section 3, we argued that such dense filaments are also traced by strong local enhancements in the ratio of bright [N II] and [S II] lines where winds encounter, compress, and shock slower gas downstream (Dopita 1997). In Section 2, we demonstrated that the ratio of two F658N images separated by 11 yr (Figure 2(c)) serves as an image filter that reveals thin bright features as local pressure gradients act to change their loci. Here we provide plausibility that enhancements in the [N II]/[S II] ratio (Figure 2(f)) trace high-density features in the electron density regime $n_e \ge 10^4$ cm⁻³, as asserted in Section 3. (The details will be published separately.)

We constructed the [N II]/[S II] ratio image with the prior expectation that the N^+/S^+ lines would arise in nearly identical volumes with the same N/S abundances, internal extinctions, and volume-filling factors, as illustrated in other PNe. In this case, the ratio image should be constant, as it is in hundreds of locations throughout the bright PN NGC 7009 (Akras et al. 2022). However, localized ratio enhancements exceeding factors of 3 of 4 are found everywhere in NGC 6302, including its high-ionization core where lines of He⁺⁺ and O⁺⁺ reach their highest surface brightnesses. (In such zones, the N^+/N and S^+/S abundance ratios $\ll 10^{-2}$; e.g., Osterbrock & Ferland 2006, Figure 2.6.)

Conceptually, we attribute the prominent enhancements in [N II]/[S II] ratio to a combination of (1) large and locally variable densities in thin, dense post-shock recombination zones and (2) the diverse ranges of critical densities, $n_{\rm crit}$, of the [N II] λ 6584, [S II] λ 6717 and λ 6731 transitions. Specifically, the [S II] λ 6717 and λ 6731 lines (2 D to 4 S transitions), $n_{\rm crit}$ is 1500 and 16,000 cm $^{-3}$, respectively. On the other hand, $n_{\rm crit}$ is 77,000 cm $^{-3}$ for the 6584 Å line (1 D₂ to 3 P transition; Draine 2011). Values of this ratio as a function of density will be more fully explored in a future paper.

ORCID iDs

Bruce Balick https://orcid.org/0000-0002-3139-3201 Joel H. Kastner https://orcid.org/0000-0002-3138-8250

¹⁵ See also Bear & Soker (2017), Glanz & Perets (2021b), and Hamers et al. (2022).

Eric Blackman https://orcid.org/0000-0002-9405-8435 Paula Moraga Baez https://orcid.org/0000-0002-1042-235X

References

```
Akras, S., Monteiro, H., Walsh, J. R., et al. 2022, MNRAS, 512, 2202
Aller, L. H., Ross, J. E., Omara, B. J., & Keyes, C. D. 1981, MNRAS, 197, 95
Balick, B., Frank, A., & Liu, B. 2019, ApJ, 877, 30
Balick, B., Frank, A., Liu, B., & Corradi, R. 2018, ApJ, 853, 168
Bally, J., Ginsburg, A., Forbrich, J., & Vargas-González, J. 2020, ApJ,
  889, 178
Barral, J. F., & Cantó, J. 1981, RMxAA, 5, 101
Barral, J. F., Cantó, J., Meaburn, J., & Walsh, J. R. 1982, MNRAS, 199, 817
Bear, E., & Soker, N. 2017, ApJL, 837, L10
Bollen, D., Kamath, D., Van Winckel, H., et al. 2022, A&A, 666, A40
Bujarrabal, V., Castro-Carrizo, A., Alcolea, J., & Sánchez Contreras, C. 2001,
     &A, 377, 868
Casassus, S., Roche, P. F., & Barlow, M. J. 2000, MNRAS, 314, 657
Contini, M., Angeloni, R., & Rafanelli, P. 2009, MNRAS, 396, 807
Davis, C. J., Smith, M. D., Stern, L., et al. 2003, MNRAS, 344, 262
De Marco, O., Akashi, M., Akras, S., et al. 2022, NatAs, 6, 1421
Dinh-V-Trung, Bujarrabal, V., Castro-Carrizo, A., et al. 2008, ApJ, 673, 934
Dopita, M. A. 1995, Ap&SS, 233, 215
Dopita, M. A. 1997, ApJ, 485, L41
Dopita, M. A., Ali, A., Karakas, A. I., et al. 2018, MNRAS, 475, 424
Dopita, M. A., & Sutherland, R. S. 1996, ApJS, 102, 161
Draine, B. T. 2011, Physics of the Interstellar and Intergalactic Medium
   (Princeton, NJ: Princeton Univ. Press)
Dupree, A. K., Strassmeier, K. G., Calderwood, T., et al. 2022, ApJ, 936, 18
Erkal, J., Nisini, B., Coffey, D., et al. 2021, ApJ, 919, 23
Fang, X., Zhang, Y., Kwok, S., et al. 2018, ApJ, 859, 92
Feibelman, W. A. 2001, ApJ, 550, 785
Forbes, D. A., & Ward, M. J. 1993, ApJ, 416, 150
García-Díaz, M. T., López, J. A., García-Segura, G., et al. 2008, ApJ, 676, 402
García-Segura, G., Taam, R. E., & Ricker, P. M. 2022, MNRAS, 517, 3822
Glanz, H., & Perets, H. B. 2021a, MNRAS, 500, 1921
Glanz, H., & Perets, H. B. 2021b, MNRAS, 507, 2659
Gómez-Gordillo, S., Akras, S., Goncalves, D. R., & Steffen, W. 2020,
   MNRAS, 492, 4097
Guerrero, M. A., Villaver, E., Manchado, A., et al. 2000, ApJS, 127, 125
Hamers, A. S., Glanz, H., & Neunteufel, P. 2022, ApJS, 259, 25
Hartigan, P., Morse, J. A., & Raymond, J. 1994, ApJ, 436, 125
Heckman, T. M. 1980a, A&A, 87, 142
Heckman, T. M. 1980b, A&A, 87, 152
Henney, W. J., López, J. A., García-Díaz, M. T., & Richer, M. G. 2021,
   MNRAS, 502, 1070
Höfner, S., & Olofsson, H. 2018, A&ARv, 26, 1
```

```
Huarte-Espinosa, M., Frank, A., Balick, B., et al. 2012, MNRAS, 424, 2055
Icke, V., Balick, B., & Frank, A. 1992, A&A, 253, 224
Jadlovský, D., Krtička, J., Paunzen, E., & Štefl, V. 2023, NewA, 99, 101962
Kastner, J. H., Montez, R. J., Balick, B., et al. 2012, AJ, 144, 58
Kastner, J. H., Moraga Baez, P., Balick, B., et al. 2022a, ApJ, 927, 100
Kastner, J. H., Moraga Baez, P., Balick, B., et al. 2022b, ApJ, 935, 180
Kastner, J. H., Weintraub, D. A., Gatley, I., et al. 1996, ApJ, 462, 777
Keohane, J. W., Reach, W. T., Rho, J., & Jarrett, T. H. 2007, ApJ,
Lago, P. J. A., & Costa, R. D. D. 2016, RMxAA, 52, 329
Lago, P. J. A., Costa, R. D. D., Faúndez-Abans, M., & Maciel, W. J. 2019,
         S, 489, 2923
Lee, C.-F., & Sahai, R. 2003, ApJ, 586, 319
López, J. A., García-Segura, G., Richer, M. G., & Steffen, W. 2008, ApJ,
Matsuura, M., Zijlstra, A. A., Molster, F. J., et al. 2005, MNRAS, 359, 383
McCray, R., & Fransson, C. 2016, ARA&A, 54, 19
Meaburn, J., Lloyd, M., Vaytet, N. M. H., & López, J. A. 2008, MNRAS,
  385, 269
Meaburn, J., López, J. A., Steffen, W., et al. 2005, AJ, 130, 2303
Meaburn, J., & Walsh, J. R. 1980a, MNRAS, 191, 5
Meaburn, J., & Walsh, J. R. 1980b, MNRAS, 193, 631
Noll, K. 2009, HST Proposal 11504
Oliva, E., Pasquali, A., & Reconditi, M. 1996, A&A, 305, 21
Osterbrock, D. E., & Ferland, G. J. 2006, Astrophysics of Gaseous Nebulae
  and Active Galactic Nuclei (2nd ed.; Mill Valley, CA: Univ. Science
Pittard, J. M., Dobson, M. S., Durisen, R. H., et al. 2005, A&A, 438, 11
Raga, A. C., Riera, A., Mellema, G., et al. 2008, A&A, 489, 1141
Raga, A. C., Steffen, W., & González, R. F. 2005, RMXAA, 41, 45
Rauber, A. B., Copetti, M. V. F., & Krabbe, A. C. 2014, A&A, 563, 42
Rechy-García, J. S., Guerrero, M. A., Duarte Puertas, S., et al. 2020, MNRAS,
  492, 1957
Reed, D. S., Balick, B., Hajian, A. R., et al. 1999, AJ, 118, 2430
Sahai, R., Bujarrabal, V., Quintana-Lacaci, G., et al. 2023, ApJ, 943, 110
Santander-García, M., Bujarrabal, V., Alcolea, J., et al. 2017, A&A, 597, A27
Soker, N., & Kashi, A. 2012, ApJ, 746, 100
Steffen, W., Koning, N., Wenger, S., Morisset, C., & Magnor, M. 2011,
  ITVCG, 17, 454
Steffen, W., & López, J. A. 2004, ApJ, 612, 319
Szyszka, C., Zijlstra, A. A., Walsh, J. R., et al. 2011, MNRAS, 416, 715
Toalá, J. A., & Arthur, S. J. 2011, ApJ, 737, 100
Toalá, J. A., & Arthur, S. J. 2014, MNRAS, 443, 3486
Toalá, J. A., & Arthur, S. J. 2018, MNRAS, 478, 1218
Walton, N. A., Walsh, J. R., & Pottasch, S. R. 1993, A&A, 275, 256
Wright, N. J., Barlow, N. J., Ercolano, B., & Rauch, T. 2011, MNRAS,
Zou, Y., Frank, A., Chen, Z., et al. 2020, MNRAS, 497, 2855
```